Journal of Materials Chemistry C

Accepted Manuscript

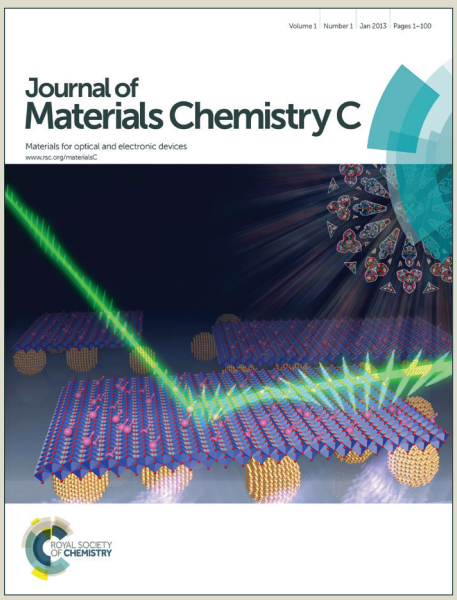

ROYAL SOCIETY OF CHEMISTRY

www.rsc.org/materialsC

A Route to Low Temperature Growth of Single Crystal GaN on Sapphire

*Pouyan Motamedi, Neda Dalili, and Kenneth Cadien**

Dr. P. Motamedi and Prof. K.C. Cadien
Department of Chemical and Materials Engineering
University of Alberta
Edmonton, Alberta, Canada T6G 2V4
E-mail: kcadien@ualberta.ca

Dr. N. Dalili
National Institute for Nanotechnology
Edmonton, Alberta, Canada T6G 2M9

Keywords: GaN, ALD, Epitaxy, XRD, Low temperature

Abstract

Gallium nitride (GaN) is considered one of most important semiconductor materials for the 21st century due to its combination of properties (high breakdown field, high electron saturation velocity and mobility, and good thermal conductivity) that make it suitable for high power, high frequency and high temperature applications. In this paper we demonstrate a possible route for the deposition of single crystal GaN on sapphire at 275°C using plasma enhanced atomic layer deposition. TEM images and electron diffraction show that the first 5 nm of growth is epitaxial then transitions to 3D growth. The films have a preferential (002) growth direction, and a small in-plane and out-of-plane misorientation. The refractive index, extinction coefficient, and optical band gap are on par with those of GaN films grown at higher temperatures. The films are p-type with a carrier concentration of 1.68×10^{18} cm^{-3} and hole mobility of 110 cm^{2}v^{-1}s^{-1}.

1. Introduction

GaN-based materials have tunable direct band gaps in the UV to IR wavelengths range, which makes them an attractive choice for cost-effective high-performance opto-electonic devices such as light emitting diodes (LEDs) and laser diodes (LDs) [1,2]. High quality GaN thin films are routinely grown by MOCVD and MBE [3–5].

In MOCVD and conventional versions of MBE, a high deposition temperature (>800°) is required to overcome the energy barriers to precursor adsorption and surface adatom migration [5–8]. However, there are certain limitations associated with deposition methods that require high temperatures. For example, these methods cannot be used for deposition of In-rich III-N materials, due to the low vapor pressure and dissociation temperature of InN [9]. This limits the potentials of III-N heterostructures in multi-junction solar cells, in which alternation between a wide band gap (In-rich) and relatively narrow band gap (Ga-rich) layers is a key structural component [10]. Furthermore, on cooling from high deposition temperatures, the large differences between the coefficient of thermal expansion of GaN and that of the common substrates, e.g. sapphire and Si, leads to a large biaxial stress, which affects the optical performance of the films [11], and may also lead to cracking and substrate bowing. Usually a thick (~25-50 nm) buffer layer is introduced between GaN and the substrate, in order to relax this stress. The necessity of this layer limits the application of high-temperature GaN films. In addition, deposition of III-N materials on flexible polymeric substrates through MOCVD and MBE is impossible [12]. Moreover, high temperature window of MOCVD (950°-1050° C) degrades the performance of Si CMOS devices, and this deposition method cannot be used for integration of III-N materials with Si CMOS technology [13].

There are few reports on the low-temperature growth of GaN on commercial substrates without the use of complex buffer layers like ZrB_2 [14] or $ScAlO_3$ [15]. Mueller et al. [16] introduced energetic neutral atom-beam lithography/epitaxy method, which is reportedly capable of depositing polycrystalline GaN at 500°C. Shin et al. [17] reported growth of GaN on MOCVD-grown GaN templates at 500° and 550°C using radio frequency plasma-assisted molecular beam epitaxy. Golgir et al. [18] have recently reported deposition of highly c-oriented GaN on sapphire using laser-assisted MOCVD. No data on the electrical and optical properties of the films have been presented.

It has been reported that deposition of epitaxial GaN films with (002) orientation, which is preferred for device applications[19,20], requires substrate temperatures higher than 600°C [21–25]. For instance, Yadav et el. [25] deposited GaN films via radio frequency sputtering, and investigated the dependence of GaN crystal structure on substrate temperature. They

reported that below 300°C the films were mostly amorphous while between 300° and 550°C the films were polycrystalline with (100) preferential orientation. The desired preferential orientation of (002) was only achieved at 700°C. Knox-Davies et al.[26] reported on the deposition of GaN via reactive sputtering at temperatures ranging from room temperature to 450°C with predominantly wurtzite polycrystalline films.

Although atomic layer deposition (ALD) may offer a potential alternative for low-temperature deposition of GaN, the extent of literature on ALD of GaN is very limited. Kim et al.[27] have reported ALD of GaN, at 650°C, using $GaCl_3$ and NH_3, leading to polycrystalline films having (002) preferential orientation with a broad XRD peak. Using halide precursors, however, may lead to film contamination[27] and pose the threat of corrosion of metal contacts[28]. On the other hand, it has been reported that low-temperature deposition of GaN using trimethylgallium and NH_3 plasma resulted in amorphous GaN films with large amounts of impurities [29]. Ozgit et al.[29,30] have reported that deposition of GaN using a conventional inductive plasma source produces amorphous films. However, using a hollow cathode plasma, they managed to deposit GaN films with (002) preferential orientation, which incongruously is reported to have been observed on Si (100), but not on sapphire (002).

In this paper, we report on the deposition of highly oriented (002) GaN on sapphire using triethylgallium (TEG) and 95% nitrogen/5% hydrogen plasma at 275°C. The hydrogen composition of the forming gas was chosen based on an estimate of quantity of hydrogen atoms needed to reduce the ethyl groups during the second ALD half reaction. The structural, optical and electrical properties of these films have been investigated using X-ray diffraction (XRD), X-ray reflectometry (XRR), atomic force microscopy (AFM), transmission electron microscopy (TEM), X-ray photoelectron spectroscopy (XPS), spectroscopic ellipsometry, and Hall Effect measurements. HRTEM observations indicate that, not only do the films have a preferred (002) orientation, they are actually epitaxial for the first ~5 nm of growth. Epitaxial growth of GaN at such a low temperature is an unprecedented observation.

2. Experiments

Depositions were carried out using an atomic layer deposition research system (ALD-150LX, Kurt J. Lesker) equipped with an in situ J. A. Woollam M-2000DI ellipsometer with a fixed angle of 70°. Depositions were carried out at 275°C using a cycle that consisted of four consecutive pulses: 0.02s TEG dose, 7s Ar purge, 15s N2/H2, 5s Ar purge, repeated for 1000 cycles to deposit a film ~55 nm thick. All depositions were done on sapphire substrates C-Plane (0001) orientation with M- axis 0.2±0.1 deg off and A- axis 0±0.1 deg off. A Kratos

AXIS Ultra XPS system was used to study the chemical structure of the films, using Al (1486.69eV) x-ray source at 50° incidence angle. An argon sputtering ion gun working at 4 KeV was used to clean the surface prior to collection of the XPS data. XRR and XRD measurements were performed using a Bruker-AXS D8-Discover machine with a Cu Kα source (Kα2 was removed before analysis). XRD data were collected using a Vantec 500 2-D detector and GADDS software, and analyzed using EVA software. XRR data and azimuthal scans were recorded using a NaI scintillometer. Commander D8 and Leptos programs were used for data acquisition and analysis, respectively. A Bruker Dimension-Edge AFM system was used to map the sample surface. Silicon tips were used in tapping mode, and the amplitude set point was 2.4 V. AFM results were analyzed using Bruker Nanoscope Analysis 1.5 software.

The structure and morphology of the ALD GaN films were characterized by TEM observation. High resolution TEM (HRTEM) was performed in a Hitachi HF 3300 instrument operated at 300kV. Cross-section TEM samples were prepared using a Hitachi NB 5000 dual beam FIB/SEM. To minimize ion beam damage to the surface of the top layer (GaN), a 50 nm layer of C was deposited on GaN surface prior to FIB processing. Bulk milling of the sample was performed using a 40 keV Ga+ beam. Final polishing was done using a 10 keV Ga+ beam. The approximate thickness of the final lamellae, mounted on Cu grids, was 100 nm. Hall Effect measurements were done using a Nanometrics HL5500 system, which was operated at 0.01 μA constant current. Optical transmission data were collected using a Perkin-Elmer LAMBDA 1050 UV/Vis/NIR spectrophotometer.

3. Results and Discussion

3.1. Composition

The XPS spectrum of a GaN film after ~5 nm of the film surface was argon ion sputter etched to remove any organic or atmospheric post-deposition contamination is shown in Fig. 1. In addition to Ga XPS peaks, Ga Auger peaks, and the nitrogen XPS peak, those from O 1s and C 1s are present. The carbon is due to remnants of the ethyl groups in the TEG precursor, and its presence indicates some degree of incomplete reaction between the nitrogen plasma and the chemically adsorbed TEG. As will be discussed in Section 3.4, carbon acts as an acceptor in GaN, and contributes to p-type conductivity. Oxygen is also an impurity that affects the electrical and optical properties of GaN [31,32]. The presence of oxygen has been well documented and reported in III-N thin film growth, especially when the growth process involves a plasma [18,27,29,33,34]however the source of this impurity is not yet fully understood.

Table 1 lists the elemental composition of the film, obtained by XPS. Gallium and nitrogen atomic fractions are almost equal, while 2.5 at.% oxygen and 1.1 at.% carbon are detected. When compared to industry-standard high-temperature MOCVD, these can be regarded as high O and C impurities. However, in comparison with recent reports of low-temperature growth of GaN, which show carbon concentrations as high as 26 at.%[18], and extremely non-stoichiometric Ga:N ratio[30], these XPS results can be considered significant.

Table 1: Elemental composition of the GaN films, as determined by XPS

Element	**Gallium**	**Nitrogen**	**Oxygen**	**Carbon**
Representative subshell	Ga 3d	N 1s	O 1s	C 1s
Atomic fraction	48.8	47.6	2.5	1.1

The AlN literature suggests that, at low concentrations of oxygen, the Al and O atoms inside the AlN lattice form Al_2O_3[35]. Recent XPS research[36] confirms that the oxidation state of Al bonded to oxygen is the same as that in Al_2O_3. Extending this concept to GaN, and assuming that every three oxygen atoms replace two nitrogen atoms in a stoichiometric compound, study of Table 1 reveals the existence of ~0.6 at.% gallium vacancy (2.5% oxygen is equivalent to 1.6%N, therefore in total there are 49.2% anions and 48.8% cations). It is known that Ga vacancies have a strong tendency to react with oxygen, and deposit at the base of edge dislocations [31]. The combination of these defects will affect the optical properties of GaN [32,37,38], and is likely to be partially responsible for the deviation of the optical properties of the films from those of the bulk material, as explained later. This hypothesis agrees well with the results of Hall mobility measurements that show a strong possibility of oxygen overcompensation by Ga vacancies. This will be discussed later.

3.2. Structure

XRR results for two different 2θ ranges are shown in Fig. 2. In Fig. 2a, the low-angle range, the reflected intensity shows a drop indicating the onset of x-ray penetration into the sample and the limit of total external reflection, also known as the critical angle. Since it is difficult to obtain a precise critical angle from the plot in Fig. 2a, minimum of the second derivative of the intensity was chosen as the point of deflection, and the onset of X-ray penetration. This method, shown in the inset of Fig. 2-a, gives a value of 0.32° for the critical angle. Bulk single crystal GaN is known to have a theoretical critical angle of 0.36°. Considering the relationship of $\theta_c \propto \sqrt{\rho}$ [39] one can estimate the density of the film to be ~95% of the theoretical value. The higher-angle XRR data in Fig. 2-b show the characteristic reflectometry

spectrum of single-layer thin films. A simulation using a genetic algorithm was run to model the film parameters. The RMS value of 3.1 nm for roughness, from atomic force microscopy, was input in the model. The data from simulation agree well with the experimental data. Simulation, run using Bruker Leptos software, gave the values of 55.6 nm and 6.08 g/cm^3 for thickness and mass density, respectively, the latter of which equals 98% of the theoretical value of bulk material. Evaluation of Kiessig fringes is a more accurate measure of density, compared to critical angle, as it takes into account the surface roughness. Nevertheless, the two methods independently give high values for the density of the film. As mentioned earlier, an in-situ ellipsometry system was used to monitor the deposition. A Cody-Lorentz model was found to offer a good description of the material's optical behavior. As was the case in XRR, a roughness value of 3.1 nm measured by AFM was input to the model. The derived value for thickness is 53.2 nm, which is ~4% lower than what was obtained from XRR.

A coupled scan XRD spectrum of the GaN PEALD film is shown in Fig. 3-a. Only two peaks at 34.5° and 41.7° (d-spacings 0.27 and 0.23 nm) are observed in the spectrum, which correspond to those of wurtzite GaN (002) and sapphire (006) reflections respectively. The absence of wurtzite GaN (100) and (101) reflections may be indicative of a single crystal or strongly oriented polycrystalline film with (002) preferred orientation. The FWHM of the GaN peak is 21.0 arc min, compared to 16.5 arc min for that of the single-crystal sapphire substrate. FWHM is related to crystallite size, and is an indicator of crystal order. The fact that the two numbers are comparable, is indicative of the high crystal quality of the GaN film. In order to probe the degree of out-of-plane tilting of crystals, a two-dimensional Hi-Star x-ray detector was employed. The rotation axes relative to the sample and the beam are schematically illustrated in Fig. 3-d. If the conventional out-of-plane rotation is denoted by ω (in a coupled scan, such as the one shown in Fig. 3-a, ω=2θ) and φ indicates the degree of in-plane rotation, then χ measures the out-of-plane rotation, whose axis is perpendicular to ω and φ rotations. The detector used in this study allows for simultaneous data collection for wide ranges of 2θ and χ [40]. Fig. 3b shows a GADDS frame centered at 2θ=34.5°. Data collection time was ten times higher than it was for Fig. 3a. It is expected that random out-of-plane orientation make cones of diffracted x-rays, which are detected as rings of uniform radial intensity distribution [41]. Therefore the degree of radial nonuniformity is a measure of crystal order [42,43]. It is clear from Fig. 3b that the film exhibits a high degree of order, while the 600-second-long collection time allows for detection of diffraction by (101) plane, whose intensity is negligible compared to that of the dominant (002) diffraction. Fig. 3-b shows an integration of the signals over 2θ, in the range of 33.5-35.5°, along χ, which confirms the narrow

distribution of the diffracted beam. Figs. 3a and 3b, in combination, provide a clear evidence that the structure of the GaN films consists of highly ordered wurtzite crystals oriented along the (002) crystallographic axis.

In thin films with strong preferential orientation, the diffraction intensity of the planes parallel to the surface is extremely sensitive to sample orientation. The maximum intensity is achieved when the beam vector and surface normal are exactly coplanar, and that is rarely the case in practice. The effect of this misorientation was revealed in a ϕ-scan and shown in Fig. 3-d. The higher intensity spectrum is the (006) reflection of sapphire, while the other spectrum is the (002) reflection of GaN. For the two spectra, the ω angle was set to 20.8° and 17.2° respectively, and 2θ was kept constant at twice the mentioned values, while the sample was rotated 360° around the surface normal. The two independently recorded spectra were then superimposed for comparison. The most noteworthy feature of Fig. 3c is the large variation of the recorded intensity vs ϕ. As explained earlier, this effect is caused by noncoplanarity of the beam vector and the surface normal. The exact coplanarity angle cannot be detected using a two-dimensional detector. Therefore a scintillometer was used to record the data in Fig. 3c. Another noteworthy feature of Fig. 3c is the fact that the two spectra show maxima and minima at the same ϕ values. This is an indication that the normal to the sapphire (006) plane and GaN (002) plane are aligned. In other words, this is proof of crystallographic relationship between the two lattices, and a sign of epitaxy at the interface.

3.3. Growth Mechanism

Cross-sectional transmission electron microscopy images of the samples are shown in Fig. 4. Ion beam damage, due to the final polishing step of sample preparation by FIB, is evident in all TEM images. Fig. 4a shows that the films have a polycrystalline structure with an epitaxial layer of ~5 nm at the sapphire interface. Fig. 4b shows this epitaxial layer in greater detail. To identify the structure of this epitaxial layer, convergent beam electron diffraction (CBED) analysis was performed. An example of a CBED pattern, shown in Fig. 4c, reveals a single crystal array of spots which can be indexed to the [110] zone axis of wurtzite GaN. Furthermore, the lattice fringes in Fig. 4b correspond to the GaN c-plane interplanar distance, indicating the epitaxial layer is c-plane oriented.

In general, two growth scenarios can be hypothesized to explain this structure. The first scenario is the coalescence of epitaxial islands with low misorientation that gives rise to a single crystal layer [44,45]. The other explanation is a transition from layer by layer to 3D polycrystalline growth. The second scenario, i.e. break of epitaxy, has been reported and

investigated in the literature before. Edge dislocations and impurities have been identified as the two potential sources for this phenomenon. It is known that after a 30° rotation, there is still a large lattice mismatch (~16%) between GaN and sapphire at the growth temperature [46]. This results in a large density of misfit dislocations. By studying the dislocation density of GaN layers grown on AlN, Daudin et al. [47,48] hypothesized that edge misfit dislocations act as nucleation centers, which give rise to GaN dots on top of the original epitaxial layers, and eventually lead to breakdown of epitaxy.

On the other hand, Liliental-Weber[49] demonstrated that a range of hollow crystal defects, mainly caused by impurities, are responsible for the transition of the GaN growth front from two-dimensional to three-dimensional. Oxygen was specifically mentioned as a likely candidate to cause these "nanotube" and "pinhole" defects. Oxygen atoms or clusters can arguably create regions with different atomic bonding at the surface. This accelerates the growth in energetically favorable areas, and leads to lack of homogeneity in growth rate at the growth front and birth of 3-D islands. Further accumulation of the defects aggravates this situation and increases surface roughness.

It must also be mentioned that exposure of sapphire (001) surface to nitrogen plasma has been shown to result in nitridation of the surface and formation of a thin AlN layer. This phenomenon has been confirmed using XPS[50–52], RHEED[53], and AFM[50,54]. Although we do not have experimental evidence for nitridation of the surface, considering the rich literature on this subject, it is considered as the likely scenario for promotion of epitaxial or highly c-oriented growth of GaN on sapphire. Thorough understanding of the growth mechanism needs further investigation.

In order to study the phenomenology of the growth front, the top-view topography of the samples was studied via AFM. Fig. 5a shows the tapping phase image from the surface of the GaN films. This mode of imaging maps the surface based upon the phase lag in the oscillation of the cantilever, compared to that of the original signal. The phase image provides better spatial resolution compared to standard height image, and has been previously selected for the study of the grain structure of the thin films [55,56]. Fig. 5a shows that the surface of the film consists of regularly-spaced features, whose outline is similar to the grain structure of a typical polycrystalline film. As mentioned earlier, detailed X-ray diffraction experiments indicate that these grains have low in-plane and out-of-plane misorientation. A 3D reconstruction of the sample surface, using the height data, as prepared by Bruker NanoScope Analysis software is shown in Fig. 5b. This is a visual representation of the growth front. The

arithmetic average and root mean square values for roughness are 3.1 nm and 3.9 nm respectively. Considering the fact that the film is ~56 nm thick, these values are decidedly higher than the roughness resulting from a two-dimensional growth regime [57,58]. This supports the previous proposition that the two-dimensional growth regime that creates the initial epitaxial layer was not sustainable, and later transforms into a three-dimensional island growth. Defect-induced surface inhomogeneity, in conjunction with surface mobility values lower than what is needed for a step-flow growth regime are believed to be the major reasons behind this transition.

3.4. Electrical and Optical Properties

Hall mobility measurements were done using a Nanometrics HL5500 system at 0.32 Tesla. The results show a relatively low resistivity of 0.033 Ω-cm. In addition, the films are p-type with a carrier concentration of 1.68×10^{18} cm^{-3} and carrier mobility of 110 cm^2/vs. Oxygen is a well-known donor in GaN, and is considered as one of the main sources of high donor concentration in nominally undoped GaN films [59,60]. XPS results indicate an oxygen atomic concentration of $5 \times 10^{20} cm^{-3}$. The fact that the films are p-type semiconductors in the absence of any other impurity, suggests an overcompensation of O by Ga vacancies. Positron annihilation spectroscopy, as well as theoretical calculations, have demonstrated that the two defects have a strong tendency to react and form stable complex defects with mobility considerable lower than the values observed for pure oxygen [60,61]. In addition, the fact that carbon impurities in the form of C_N has been shown to act as an acceptor [62–66] means that the carbon impurity present in the films may act as a compensation source for oxygen donors.

The refractive index and absorption coefficient were measured using spectroscopic ellipsometry, and the dispersion curves are shown in Fig. 6-a. The value of refractive index at 632 nm is 2.21, compared to 2.38 for the bulk value. Considering the porosity of 2%, as obtained by XRR, one can apply the Bruggeman effective medium approximation to calculate the expected refractive index from the bulk value. This yields a value of 2.31, which still higher than the thin film value.

In order to study the effect of structural variations on the refractive index, the results of *in-situ* spectroscopic ellipsometry were analyzed, and refractive index was derived at various depths. The results are displayed in Fig. 6-b. As observed, at ~10 nm, the decreasing trend of refractive index reverses to a rising trend. These results can be analyzed in view of the discussions presented in section 2.3. As the films have an epitaxial structure during the first few nanometers of growth, the refractive index is high and closer to that of the bulk value.

A transition from two-dimensional growth regime to three-dimensional results in higher porosity and lower crystalline quality, hence lower refractive index. Further increase in thickness yields larger crystals and lower concentration of defects, therefore higher index. While the rising trend has been reported for various semiconductors[67–69], the initial decrease is a rare observation caused by the specific structural evolution of this film.

It is known that in proximity of the band gap, semiconductors with direct optical band gaps, E_g, follow Eq. (1),

$$(\alpha h\nu)^2 \propto (E - E_g) \qquad (1)$$

where $\alpha = 4\pi k\lambda^{-1}$ is the absorption coefficient, λ is wavelength, ν is frequency, h is Plank's constant, and k is the extinction coefficient, and A is a constant related to the effective mass of holes and electrons in the semiconductor [70]. When the left hand side of the Eq. (1) is plotted as a function of photon energy ($h\nu$), the intercept of the tangent to the linear portion of the graph with the x-axis gives the approximate value of the optical band gap. In addition to ellipsometry, the absorption coefficient was also derived from spectrophotometry in transmission mode (Fig. 6-c). Fig. 6-d shows the aforementioned procedure applied to the two sets of data and the resulting band gaps. The values resulting from ellipsometry and spectrophotometry are 3.62 and 3.55 eV, respectively. The two numbers are both higher than the bulk value of 3.4 eV.

It has been documented that the thickness of thin films affects their refractive index and optical band gap [68,71–74]. In the case of CdS, it has been reported that an increase in thickness from 40 to 113 nm results in narrowing of band gap from 2.88 to 2.61 eV, while the refractive index at 632 nm increases by 0.35 [72]. In the case of CdSe, a decrease of 0.6 eV in optical band gap energy has been reported as the thickness is increased from 250 nm to 400 nm [68]. Goh et al.[75] have reported that the optical parameters of Ge films deposited by electron beam evaporation stabilize at thicknesses >20 nm[75], whereas $CuInS_2$ films deposited by thermal evaporation have been reported to reach stabilization for thicknesses >200 nm [73]. In addition, or very thin films (<15 nm), quantum confinement becomes relevant, and the energy spectrum of the two-dimensional system becomes discrete, which results in the size-dependency of the band gap [76]. However, in the case of thicker films, such as those studied in this work, the potential effect of thickness on optical parameters may be attributed to crystal disorder, caused by dislocations, stacking faults and grain boundary misorientation. The presence of acceptor-like defect bands above the valance band could also lead to effective widening of the band gap [77]. Defect states between the conduction band and valance band will

generally make the fundamental transition less probable, effectively resulting in a higher observed band gap energy [72].

4. Conclusions

We have presented compositional and structural evidence of the growth of gallium nitride thin films using atomic layer deposition at 275°C. XPS shows that the films are nearly stoichiometric with low amounts of oxygen and carbon impurities, compared to the values reported in the literature for low-temperature growth of GaN. X-ray reflectometry shows that the deposited GaN has a density equal to 98% of that of the bulk. X-ray diffraction confirmed that the films are (002)-oriented and highly ordered with low out-of-plane misorientation. Superimposed azimuthal scans of GaN (002) peak and Sapphire (006) peak show evidence of the crystallographic relationship between the film and the substrate. Cross-sectional high resolution TEM micrographs shows that the films are epitaxial for the first ~5nm, before turning polycrystalline. The combination of TEM and AFM observations reveal that the initial epitaxial growth is not sustainable, and transforms into a three-dimensional island growth regime after the first few nanometers of growth. Preliminary electrical measurements indicate that the films are p-type semiconductors with a resistivity of 0.033 Ω-cm, 1.68×10^{18} cm^{-3} carrier concentration and a carrier mobility of 110 cm^2/vs. These results have been interpreted in light of XPS stoichiometry analyses. Optical performance of the films has been evaluated using an in-situ spectroscopic ellipsometry. It is shown that the refractive index is slightly lower than the bulk value, and the amount of deviation is within the expected range for films of comparable thicknesses. A similar trend was observed for the optical band gap.

Acknowledgement

The authors (PM and KC) wish to thank Alberta Innovates Technology Futures and NSERC Discovery Grants for support of this work. We also wish to thank National Institute for Nanotechnology for the TEM work and Dr Marek Malac for support of this work. The Alberta Centre for Surface Engineering and Science is acknowledged for use of their AFM and XPS facilities.

References

1 A. Khan, K. Balakrishnan and T. Katona, *Nat. Photonics*, 2008, **2**, 77–84.

2 M. Asif Khan, M. Shatalov, H. P. Maruska, H. M. Wang and E. Kuokstis, *Jpn. J. Appl. Phys.*, 2005, **44**, 7191–7206.

3 N. H. Karam, T. Parodos, P. Colter, D. McNulty, W. Rowland, J. Schetzina, N. El-Masry and S. M. Bedair, *Appl. Phys. Lett.*, 1995, **67**, 94.

4 B. . Liu, M. Lachab, a Jia, a Yoshikawaa and K. Takahashi, *J. Cryst. Growth*, 2002, **234**, 637–645.

5 K. Kushi, H. Sasamoto, D. Sugihara, S. Nakamura, A. Kikuchi and K. Kishino, *Mater. Sci. Eng. B*, 1999, **59**, 65–68.

6 S. J. Pearton, F. Ren, a. P. Zhang and K. P. Lee, *Mater. Sci. Eng. R Reports*, 2000, **30**, 55–212.

7 P. Gibart, *Reports Prog. Phys.*, 2004, **67**, 667–715.

8 S. J. Pearton, J. C. Zolper, R. J. Shul and F. Ren, *J. Appl. Phys.*, 1999, **86**, 1.

9 Y. Nanishi, Y. Saito and T. Yamaguchi, *Japanese J. Appl. Physics, Part 1 Regul. Pap. Short Notes Rev. Pap.*, 2003, **42**, 2549–2559.

10 H. Cotal, C. Fetzer, J. Boisvert, G. Kinsey, R. King, P. Hebert, H. Yoon and N. Karam, *Energy Environ. Sci.*, 2009, **2**, 174.

11 D. G. Zhao, S. J. Xu, M. H. Xie, S. Y. Tong and H. Yang, *Appl. Phys. Lett.*, 2003, **83**, 677–679.

12 H. Jin, J. Zhou, S. R. Dong, B. Feng, J. K. Luo, D. M. Wang, W. I. Milne and C. Y. Yang, *Thin Solid Films*, 2012, **520**, 4863–4870.

13 T. E. Kazior, R. Integrated, D. Systems and L. Street, *Philos. Trans. R. Soc. A Math. Phys. Eng. Sci.*, 2013, **372**, 1–15.

14 R. a. Trivedi, J. Tolle, a. V. G. Chizmeshya, R. Roucka, C. Ritter, J. Kouvetakis and I. S. T. Tsong, *Appl. Phys. Lett.*, 2005, **87**, 85–88.

15 T. Katase, K. Nomura, H. Ohta, H. Yanagi, T. Kamiya, M. Hirano and H. Hosono, *Mater. Sci. Eng. B*, 2009, **161**, 66–70.

16 A. H. Mueller, E. a. Akhadov and M. a. Hoffbauer, *Appl. Phys. Lett.*, 2006, **88**, 1–3.

17 I. S. Shin, K. Wang, T. Araki, E. Yoon and Y. Nanishi, *Appl. Phys. Express*, 2012, **5**, 0–3.

18 H. R. Golgir, Y. Gao, Y. S. Zhou, L. Fan, P. Thirugnanam, K. Keramatnejad, L. Jiang and Y. F. Lu, *Cryst. Growth Des.*, 2014, 6248–6253.

19 F. a. Ponce, D. P. Bour, W. T. Young, M. Saunders and J. W. Steeds, *Appl. Phys. Lett.*, 1996, **69**, 337.

20 S.-H. Park and S.-L. Chuang, *J. Appl. Phys.*, 2000, **87**, 353.

21 M. Park, J.-P. Maria, J. J. Cuomo, Y. C. Chang, J. F. Muth, R. M. Kolbas, R. J. Nemanich, E. Carlson and J. Bumgarner, *Appl. Phys. Lett.*, 2002, **81**, 1797.

22 Z. S. Schiaber, D. M. G. Leite, J. R. R. Bortoleto, P. N. Lisboa-Filho and J. H. D. da Silva, *J. Appl. Phys.*, 2013, **114**, 183515.

23 B. S. Yadav, S. Singh, T. Ganguli, R. Kumar, S. S. Major and R. S. Srinivasa, *Thin Solid Films*, 2008, **517**, 488–493.

24 M. Hao, H. Ishikawa and T. Egawa, *Appl. Phys. Lett.*, 2004, **84**, 4041.

25 B. S. Yadav, S. S. Major and R. S. Srinivasa, *J. Appl. Phys.*, 2007, **102**, 073516.

26 E. C. Knox-Davies, J. M. Shannon and S. R. P. Silva, *J. Appl. Phys.*, 2006, **99**, 073503.

27 O. H. Kim, D. Kim and T. Anderson, *J. Vac. Sci. Technol. A Vacuum, Surfaces, Film.*, 2009, **27**, 923.

28 D. M. King, X. Du, A. S. Cavanagh and A. W. Weimer, *Nanotechnology*, 2008, **19**, 445401.

29 C. Ozgit, I. Donmez, M. Alevli and N. Biyikli, *J. Vac. Sci. Technol. A Vacuum, Surfaces, Film.*, 2012, **30**, 01A124.

30 C. Ozgit-Akgun, E. Goldenberg, A. K. Okyay and N. Biyikli, *J. Mater. Chem. C*, 2014, **2**, 2123.

31 J. Elsner, R. Jones, M. Heggie, P. Sitch, M. Haugk, T. Frauenheim, S. Öberg and P. Briddon, *Phys. Rev. B*, 1998, **58**, 12571–12574.

32 M. Toth, K. Fleischer and M. R. Phillips, *Phys. Rev. B*, 2007, **59**, 1575–1578.

33 M. Alevli, C. Ozgit, I. Donmez and N. Biyikli, *Phys. Status Solidi*, 2012, **209**, 266–271.

34 L. Rosenberger, R. Baird, E. McCullen, GregoryAuner and G. Shreve, *Surf. Interface Anal.*, 2008, **40**, 1254–1261.

35 J. H. Harris, R. A. Youngman and R. G. Teller, *J. Mater. Res.*, 1990, **44128**, 1763–1773.

36 P. Motamedi and K. Cadien, *Appl. Surf. Sci.*, 2014, **315**, 104–109.

37 V. . Bermudez, D. . Koleske and a. . Wickenden, *Appl. Surf. Sci.*, 1998, **126**, 69–82.

38 J. Oila, J. Kivioja, V. Ranki, K. Saarinen, D. C. Look, R. J. Molnar, S. S. Park, S. K. Lee and J. Y. Han, *Appl. Phys. Lett.*, 2003, **82**, 3433.

39 E. Chason and T. M. Mayer, *Crit. Rev. Solid State Mater. Sci.*, 1997, **22**, 1–67.

40 Bruker AXS, *General Area Detector Diffraction System (GADDS) User Manual*, Madison, WI, 4.1 edn.

41 M. Birkholz, *Thin Film Analysis by X-Ray Scattering*, Wiley, 2006.

42 S. Y. Sayed and J. M. Buriak, *ACS Appl. Mater. Interfaces*, 2010, **2**, 3515–24.

43 T. Nagata, J. Volk, M. Haemori, Y. Yamashita, H. Yoshikawa, R. Hayakawa, M. Yoshitake, S. Ueda, K. Kobayashi and T. Chikyow, *J. Appl. Phys.*, 2010, **107**, 103714.

44 V. Lebedev, K. Tonisch, F. Niebelschütz, V. Cimalla, D. Cengher, I. Cimalla, C. Mauder, S. Hauguth, O. Ambacher, F. M. Morales, J. G. Lozano and D. González, *J. Appl. Phys.*, 2007, **101**.

45 H. Choe, S. Lee, B. Shin and C. Kim, *J. Cryst. Growth*, 2008, **310**, 3278–3281.

46 S. A. Kukushkin, A. V Osipov, V. N. Bessolov, B. K. Medvedev, V. K. Nevolin and K. A. Tcarik, *Rev. Adv. Mater. Sci.*, 2008, **17**, 1–32.

47 B. Daudin, G. Feuillet, G. Mula, H. Mariette, J. L. Rouviere, N. Pelekanos, G. Fishman, C. Adelmann and J. Simon, *Phys. Status Solidi*, 1999, **621**, 621–628.

48 B. Daudin, F. Widmann, G. Feuillet, Y. Samson, M. Arlery and J. L. Rouvie, *Phys. Rev. B*, 1997, **56**, 7069–7072.

49 Z. Liliental-Weber, *J. Electron Microsc. (Tokyo).*, 2000, **49**, 339–48.

50 J.-S. Paek, K.-K. Kim, J.-M. Lee, D.-J. Kim, M.-S. Yi, D. Y. Noh, H.-G. Kim and S.-J. Park, *J. Cryst. Growth*, 1999, **200**, 55–62.

51 M. Losurdo, P. Capezzuto and G. Bruno, *J. Appl. Phys.*, 2000, **88**, 2138.

52 M. Losurdo, P. Capezzuto, G. Bruno, G. Namkoong, W. A. Doolittle and A. S. Brown, *J. Appl. Phys.*, 2002, **91**, 2508–2518.

53 F. Widmann, G. Feuillet, B. Daudin and J. L. Rouvière, *J. Appl. Phys.*, 1999, **85**, 1550.

54 N. Grandjean, J. Massies and M. Leroux, *Appl. Phys. Lett.*, 1996, **69**, 2071.

55 R. Coq Germanicus, E. Picard, B. Domenges, K. Danilo and R. Rogel, *Appl. Surf. Sci.*, 2007, **253**, 6006–6012.

56 C. H. Pang, P. Hing and a. See, *J. Vac. Sci. Technol. B Microelectron. Nanom. Struct.*, 2002, **20**, 1866.

57 D. Kapolnek, X. H. Wu, B. Heying, S. Keller, B. P. Keller, U. K. Mishra, S. P. DenBaars and J. S. Speck, *Appl. Phys. Lett.*, 1995, **67**, 1541.

58 X. H. Wu, D. Kapolnek, E. J. Tarsa, B. Heying, S. Keller, B. P. Keller, U. K. Mishra, S. P. DenBaars and J. S. Speck, *Appl. Phys. Lett.*, 1996, **68**, 1371.

59 C. Wetzel, T. Suski, J. Ager III, E. Weber, E. Haller, S. Fischer, B. Meyer, R. Molnar and P. Perlin, *Phys. Rev. Lett.*, 1997, **78**, 3923–3926.

60 K. Saarinen, V. Ranki, T. Suski, M. Bockowski and I. Grzegory, *J. Cryst. Growth*, 2002, **246**, 281–286.

61 M. Rummukainen, J. Oila, a. Laakso, K. Saarinen, a. J. Ptak and T. H. Myers, *Appl. Phys. Lett.*, 2004, **84**, 4887.

62 S. Shimizu and Saki Sonoda, in *Proc. Int. Workshop on Nitride Semiconductors*, 2000.

63 H. Tang, J. B. Webb, J. a. Bardwell, S. Raymond, J. Salzman and C. Uzan-Saguy, *Appl. Phys. Lett.*, 2001, **78**, 757–759.

64 D. J. As, U. Köhler, M. Lübbers, J. Mimkes and K. Lischka, *Phys. Status Solidi Appl. Res.*, 2001, **188**, 699–703.

65 S. Fischer, C. Wetzel, E. E. Haller and B. K. Meyer, *Appl. Phys. Lett.*, 1995, **67**, 1298–1300.

66 J. L. Lyons, a. Janotti and C. G. Van de Walle, *Phys. Rev. B*, 2014, **89**, 035204.

67 I. Chambouleyron, S. D. Ventura, E. G. Birgin and J. M. Martínez, *J. Appl. Phys.*, 2002, **92**, 3093.

68 Y. Akaltun, M. A. Yıldırım, A. Ateş and M. Yıldırım, *Opt. Commun.*, 2011, **284**, 2307–2311.

69 P. Motamedi and K. Cadien, *J. Cryst. Growth*, 2015, **421**, 45–52.

70 C. F. Klingshirn, *Semiconductor Optics*, Springer Berlin Heidelberg, Berlin, Heidelberg, 2012.

71 R. S. Reddy, *Adv. Mater. Lett.*, 2012, **3**, 239–245.

72 S. Kumar, S. Kumar, P. Sharma, V. Sharma and S. C. Katyal, *J. Appl. Phys.*, 2012, **112**, 123512.

73 M. Ben Rabeh, N. Khedmi, M. a. Fodha and M. Kanzari, *Energy Procedia*, 2014, **44**, 52–60.

74 A. Rahal, S. Benramache and B. Benhaoua, *J. Semicond.*, 2013, **34**, 093003.

75 E. S. M. Goh, T. P. Chen, C. Q. Sun and Y. C. Liu, *J. Appl. Phys.*, 2010, **107**, 024305.

76 S. V. Gaponenko, *Optical Properties of Semiconductor Nanocrystals*, Cambridge University Press, 1998.

77 A. Meeder, D. F. Marrón, A. Rumberg, M. C. Lux-Steiner, V. Chu and J. P. Conde, *J. Appl. Phys.*, 2002, **92**, 3016.

Figure Captions:

Figure 1: XPS survey spectrum of the GaN film after ion etch cleaning.

Figure 2: (a) X-ray reflectometry spectra of a 1000-cycle ALD GaN film showing the critical angle; the inset shows the method used to extract the critical angle; (b) characteristic Kiessig fringes in GaN XRR spectra.

Figure 3: (a) Coupled scan XRD spectrum of GaN on sapphire; (b) a two dimensional XRD frame of GaN on sapphire with the accompanying integration of the intensity along the χ axis; (c) superimposed azimuthal scans of sapphire (006) and GaN (002) XRD peaks; (d) the schematic illustration of the geometrical parameters of the XRD tests.

Figure 4: (a, b) High resolution transmission electron micrographs of GaN-sapphire interface; (c) convergent beam electron diffraction pattern of the epitaxial layer at the interface.

Figure 5: (a) Phase image atomic force micrograph of the surface of the GaN films; (b) a three-dimensional reconstruction of the surface contour, extracted from the AFM height sensor data.

Figure 6: (a) Variations of the refractive index and extinction coefficient, extracted from spectroscopic ellipsometry data (b) the evolution of the refractive index of GaN at 632 nm during the growth process (c) transmission spectrophotometry data for GaN films on sapphire (d) comparison of the optical band gap extracted from spectrophotometry and ellipsometry data.

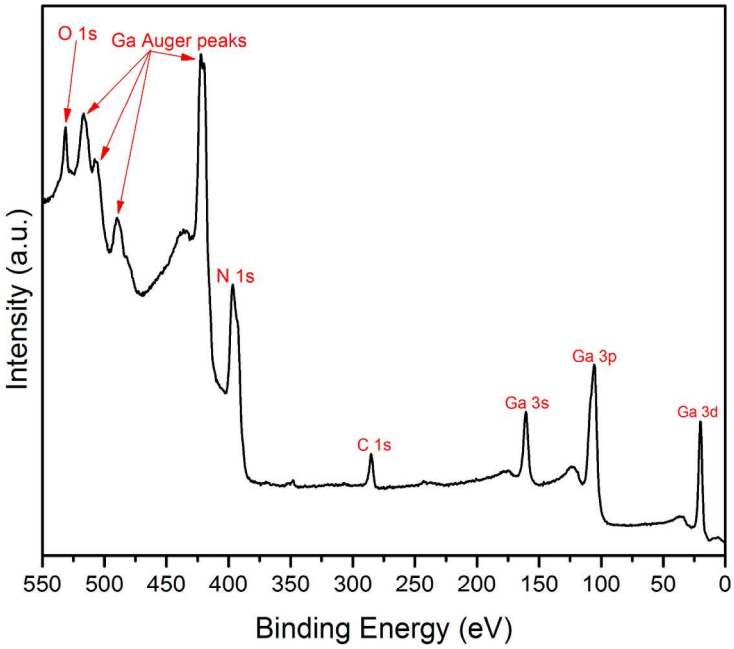

271x207mm (300 x 300 DPI)

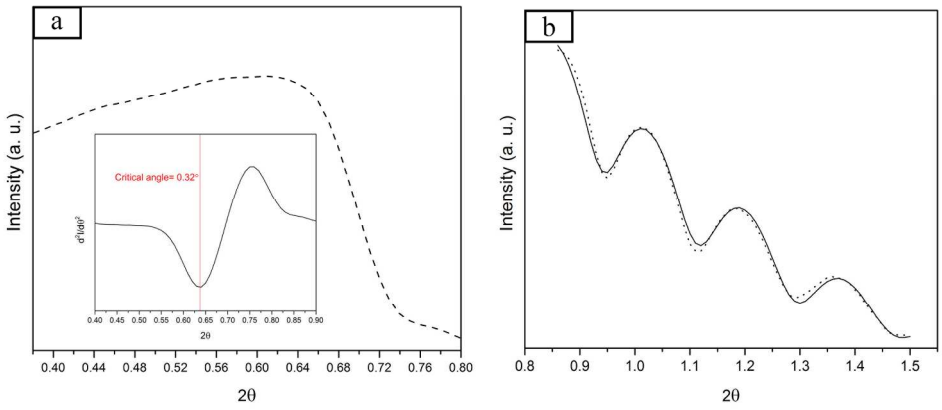

304x127mm (300 x 300 DPI)

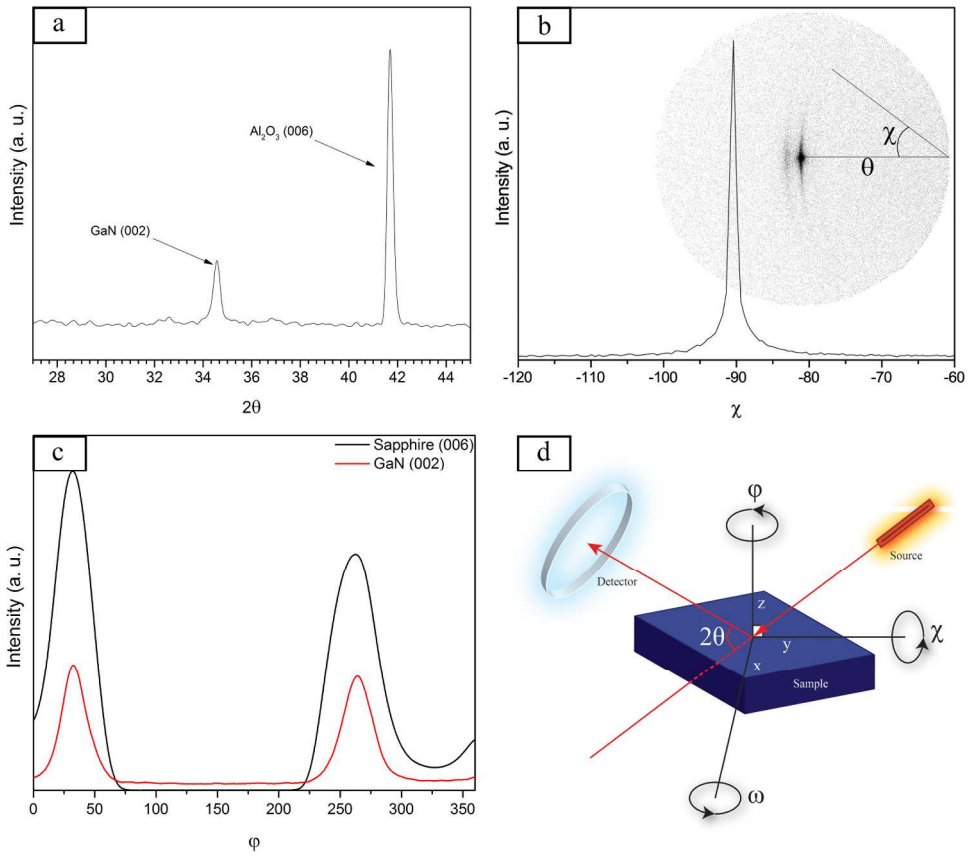

304x274mm (300 x 300 DPI)

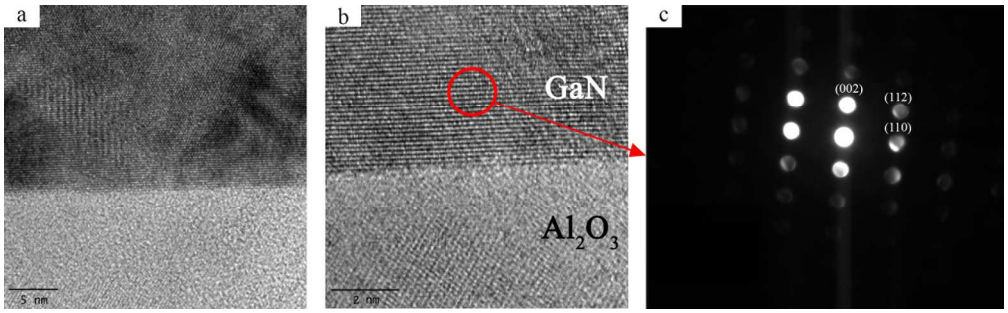

218x66mm (300 x 300 DPI)

133x60mm (300 x 300 DPI)

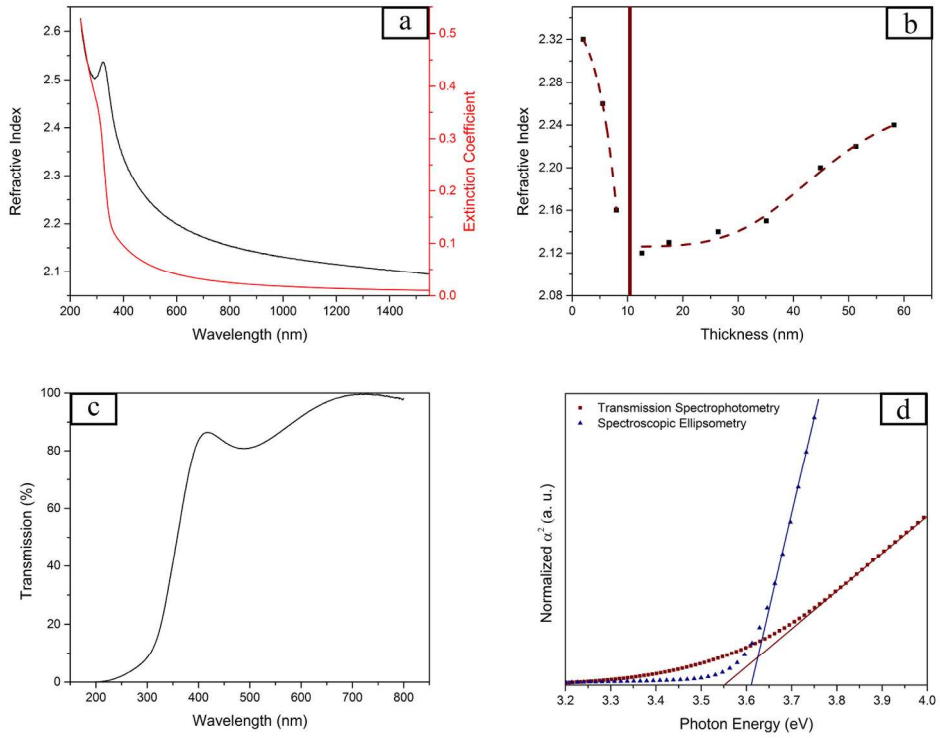

289x220mm (300 x 300 DPI)